This document contains additional information on the sediment trap data, processing of the aquatic eddy covariance (AEC) dataset, analysis of the local hydrodynamics and relationship between AEC-based fluxes and flow velocity and direction. Text S1 provides a more detailed description of the correlation between oxygen (O_2) uptake and flow characteristics (velocity magnitude and direction) depicted in Figure S3. Table S1 presents an overview of the data obtained from the sediment trap deployments as shown in Figure 4. Table S2 provides the mean characteristics of the theoretical AEC footprint area integrated by AEC measurements at the respective sites. Figure S1 shows examples of the AEC dataset for a coral garden site and the reference sandy site, and provides a visual depiction of the procedure used to identify periods of stable flux (i.e., habitats) for the garden sites as described in the Methods section. Figure S2 shows the theoretical particle track analysis for each site. Figure S3 shows the flow velocity magnitude, flow direction and O_2 uptake correlation plots for the garden sites together with the associated principal component analysis, as detailed in Text S1. Figure S4 shows local estimates of net primary production based on remote sensing and the associated flux of particulate organic carbon (POC) based on established empirical relationships (see Figure S4 caption for details).

Text S1. Coral garden site characterization from oxygen (O_2) uptake and flow characteristics

Within the coral garden sites, mean habitat O_2 uptake rates ranged from 5 to 40 mmol m^{-2} d^{-1} (Fig. 3). Compared with the global range from sedimentary habitats at similar depths (after Glud 2008), the mean habitats rates reported for AEC-2 were systematically higher, up to a factor of 4. In contrast, for AEC-3 and AEC-5, the habitats' mean uptake fell closer to the rates observed across the sandy sites, with only 2-3 habitats showing enhanced O_2 uptake rates (Fig. 3). This could be in part explained by the presence of habitats with different proportions of depositional sand and more colonized hard substrates, both across sites and within sites. While our experimental setup did not allow for a direct quantification of faunal densities and proportion of colonized areas, our benthic imaging (e.g., Fig. 1) hints at larger proportion of depositional sand at AEC-3 and AEC-5 than at AEC-2, in agreement with the observed differences in O_2 uptake (Fig. 3).

The local hydrodynamics regime was also found to modulate the observed O_2 uptake dynamics. In fact, in our principal component analysis (PCA), flow velocity magnitude and direction alone, when expresses as principal component 1, explained almost 60% of the data variance, contrasting with the ~35% of the second principal component, which was clearly identifiable as being driven by habitats-specific faunal density and habitat coverage. (Fig. 3d). Based of flow characteristics, all three sites showed a comparable flow velocity range, but AEC-2 and AEC-3 were characterized by slightly lower mean flow velocities than AEC-5 (Table 2), as also depicted visually by the site-specific particle tracks (see Fig. S2). It is thus not surprising that in the PCA, AEC-2 and AEC-3 are clustered together and spread along the second principal component while AEC-5 is clearly separated from the other two sites. It should be noted that the actual location of the sites within the summit varied very little, by less than 50 m (Fig. 1), suggesting that the differences in flow velocities and direction (see Fig. S2) may be in part due to the integration between the flow and localized small-scale topography features. Overall, our PCA, albeit limited by the reduced amount of available measurements, suggests that the benthic O_2 uptake is ultimately driven by a complex interplay between the local hydrodynamics and habitat characteristics, i.e., faunal density and habitat coverage.

Table S1. Overview of sediment trap sampling showing the integrated fluxes of particulate nitrogen (PN) and carbon (PC), particulate organic carbon (POC), particulate inorganic carbon (PIC) as well as the POC to PN ratio.

Bottle number	Opening date	Closing date	Days	PN (µmol m^{-2} d^{-1})	PC (µmol m^{-2} d^{-1})	POC (µmol m^{-2} d^{-1})	PIC (µmol m^{-2} d^{-1})	POC/PN
1	1 Dec 2017	1 Jan 2018	31	15.99	170.94	119.80	51.14	7.49
2	1 Jan 2018	1 Feb 2018	31	15.07	204.40	127.50	76.90	8.46
3	1 Feb 2018	8 Feb 2018	7	24.94	1213.58	314.95	898.63	12.63
4	8 Feb 2018	15 Feb 2018	7	37.39	330.00	250.04	79.95	6.69
5	15 Feb 2018	22 Feb 2018	7	20.71	270.10	174.29	95.81	8.41
6	22 Feb 2018	1 Mar 2018	7	40.28	387.68	214.59	173.08	5.33
7	1 Mar 2018	8 Mar 2018	7	12.29	193.80	77.39	116.42	6.30
8	8 Mar 2018	15 Mar 2018	7	23.32	211.04	155.25	55.79	6.66
9	15 Mar 2018	22 Mar 2018	7	21.47	247.39	134.37	113.02	6.26
10	22 Mar 2018	29 Mar 2018	7	110.38	898.30	709.40	188.90	6.43
11	29 Mar 2018	4 Apr 2018	7	76.27	863.06	585.00	278.06	7.67
12	4 Apr 2018	12 Apr 2018	7	85.25	834.83	625.45	209.38	7.34
13	12 Apr 2018	19 Apr 2018	7	148.40	1676.91	1238.63	438.28	8.35
14	19 Apr 2018	26 Apr 2018	7	88.63	720.50	570.07	150.43	6.43
15	26 Apr 2018	3 May 2018	7	68.44	687.71	587.03	100.67	8.58
16	3 May 2018	10 May 2018	7	61.29	832.17	498.94	333.23	8.14
17	10 May 2018	17 May 2018	7	186.82	2570.39	1601.51	968.89	8.57
18	17 May 2018	24 May 2018	7	83.26	749.61	572.77	176.85	6.88
19	24 May 2018	31 May 2018	7	42.84	424.12	326.40	97.71	7.62
20	31 May 2018	7 Jun 2018	8	27.41	221.31	198.58	22.73	7.24

Table S2. Characteristics of the theoretical footprint area integrated by the aquatic eddy covariance for each site based on the model parametrization by Berg et al. (2007). It shows the mean bottom roughness length scale (z_0), the footprint length (F_{length}) and width (F_{width}), region of maximum flux contribution (X_{max}) and overall footprint area (F_{area}) for each site. Note that the model was applied outside of the validated range (z_0 ≤ 1 cm and measurement height ≤ 0.3 m). The resulting footprint estimates might therefore be subject to higher uncertainties.

Site	AEC Deployment	z_0 (cm)	F_{length} (m)	F_{width}[a] (m)	X_{max} (m)	F_{area}[b] (m^2)
Sand	AEC-1	0.8	56.9	2.3	2.4	102.2
Sand (off garden)	AEC-4	4.5	22.1	2.3	0.6	39.7
Coral garden	AEC-2	6.4	11.6	2.3	0.13	20.9
Coral garden	AEC-3	6.8	12.4	2.3	0.1	22.3
Coral garden	AEC-5	7.3	8.2	2.3	0.04	14.7

a: for a measurement height (h) of 0.35 m
b: approximated as an ellipsoid.

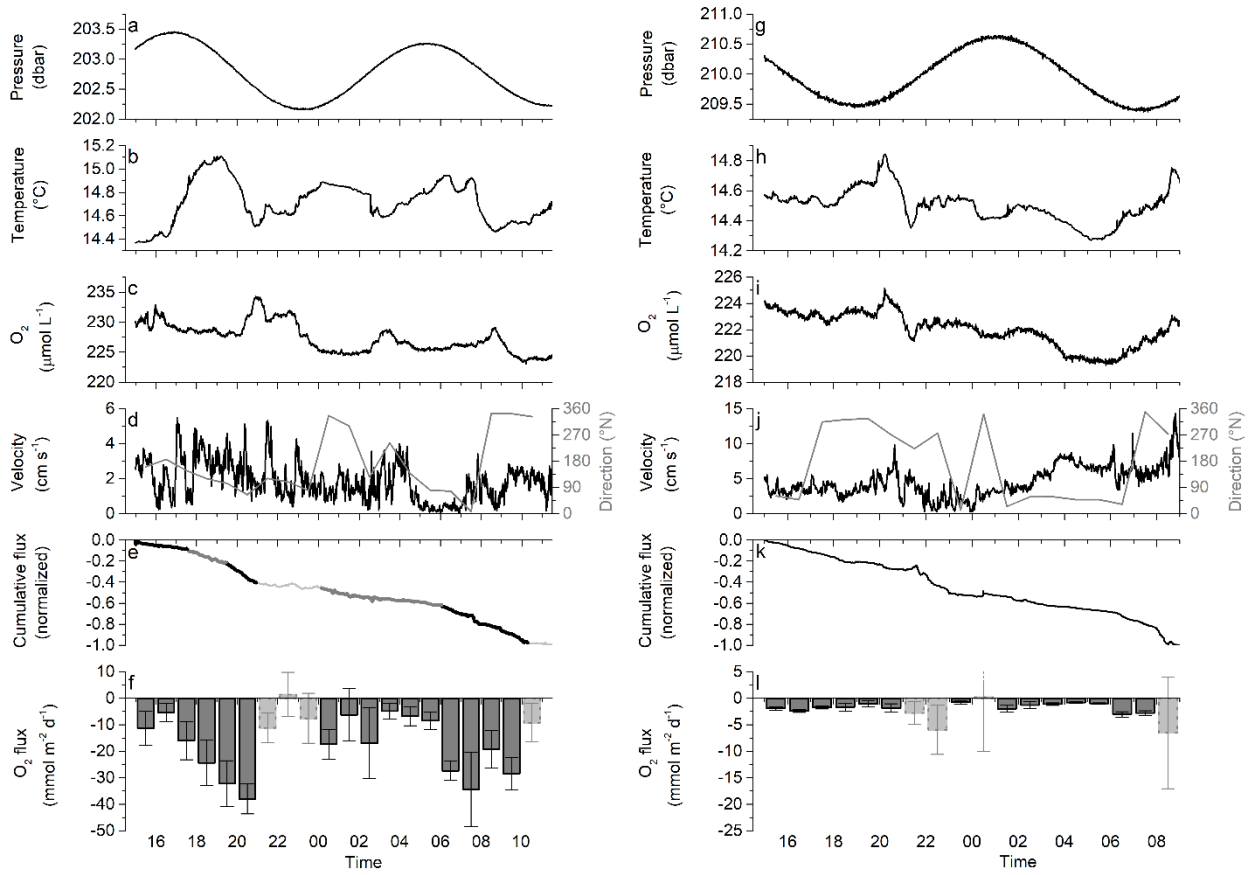

Figure S1. Example of aquatic eddy co-variance (AEC) dataset for the mixed coral garden (AEC-2; a – f) and sandy reference site (AEC-1; g – l). It shows time series of pressure (a, g), temperature (b, h), dissolved oxygen (O_2; c, i) from the SBE19 CTD probe, flow velocity and flow direction (gray line) from the acoustic Doppler velocimeter (d, j). Panels e, k, depict the normalized cumulative flux; periods with stable linear changes in the cumulative flux were used to characterized coral garden habitats, as exemplified by the grey and black lines in panel e (see Figure 3). Hourly O_2 flux averages with standard error are shown in panels f and l; averages from periods with unstable cumulative flux (light grey bars) were flagged and not included on the site's averages (see Table 2). Note that the observed correlation between temperature and O_2 during deployment AEC01 (panels h, j) and AEC03 (not shown) might have affected the obtained O_2 uptake. Given the reduced O_2 concentration changes over the deployment, however, the effect was deemed negligible.

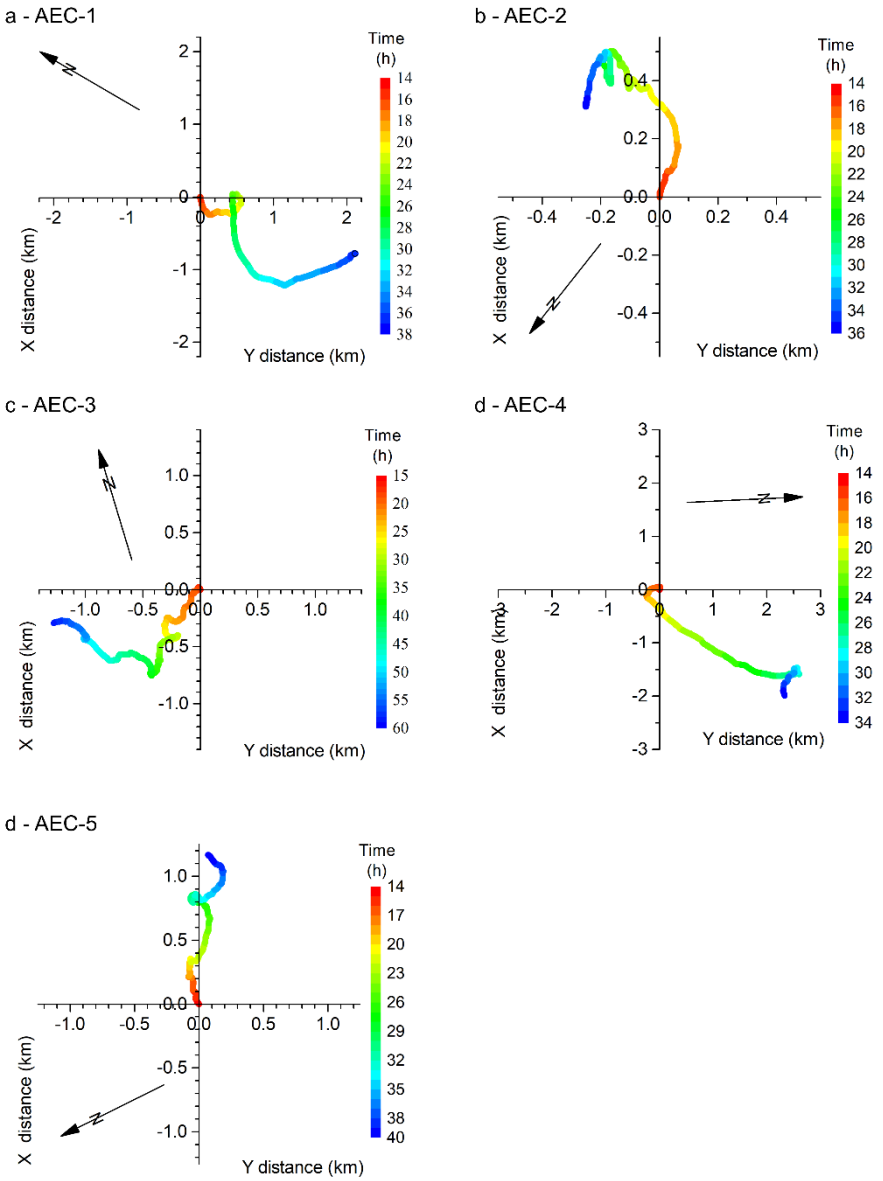

Figure S2. Theoretical two-dimensional particle track analysis for all AEC deployments. The travel distance along the ADV instrument coordinates X and Y are plotted at 1 min interval with the tracks color representing the deployment time in hours (starting at 00:00 of each deployment day). The arrows indicate the North direction in relation to the instrument coordinate system.

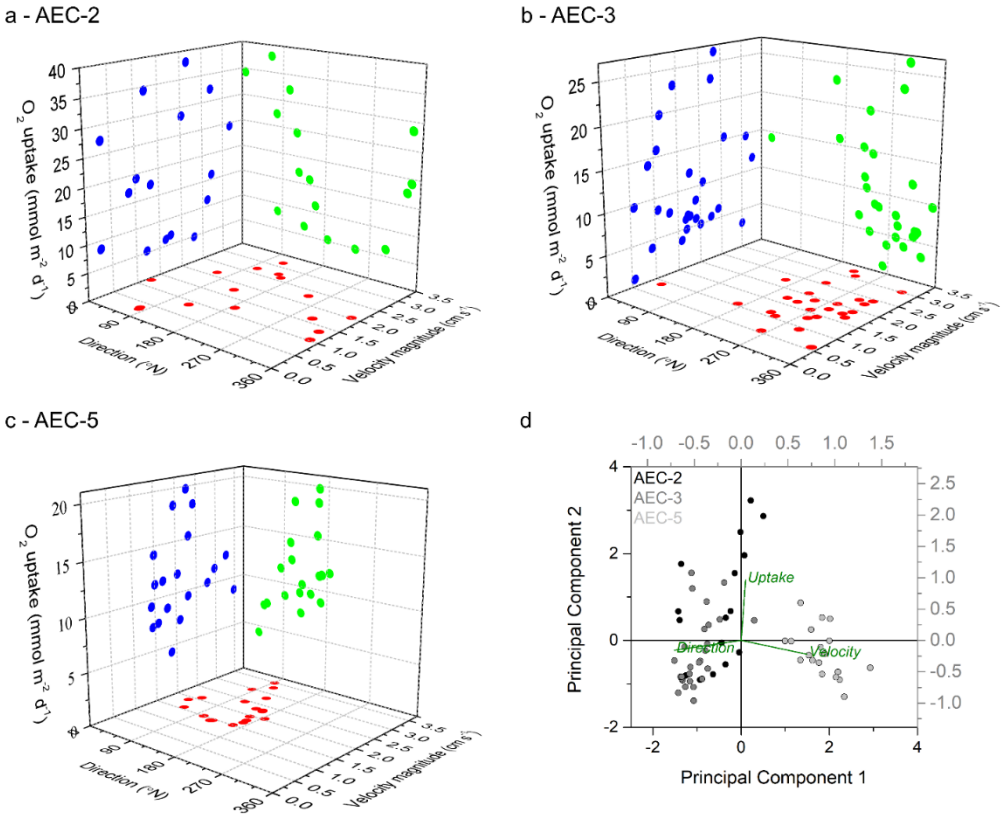

Figure S3. Correlation between O_2 uptake rates and flow velocity magnitude and direction. It shows three-dimensional correlation plots for AEC-2 (a), AEC-3 (b), and AEC-5 (c) based on hourly O_2 uptake averages and associated flow characteristics. (d) Correlation-based principal components analysis of the data shown on panels a-c. Note that the principal component 1 (PC1) is mostly driven by hydrodynamics, with principal component 2 (PC2) being mostly driven by changes in O_2 uptake. PC1 and PC2 explained 58.3% and 35.3% of the data variance, respectively.

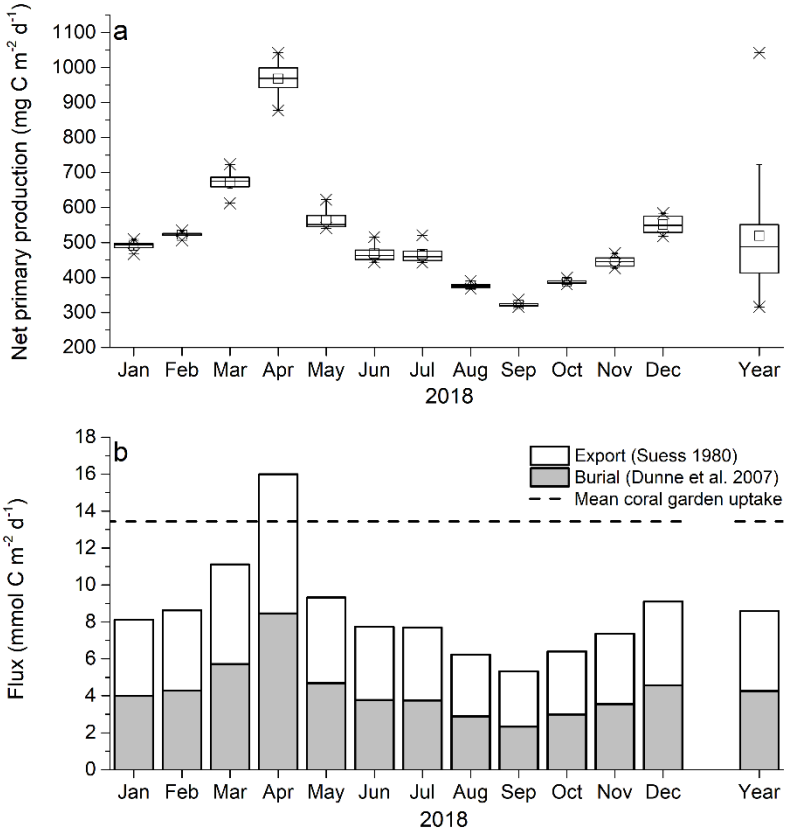

Figure S4. (a) Mean monthly estimates of net primary production (NPP) within the Condor seamount region (latitude 38° 27' to 38° 36' N and longitude 28° 51' to 29° 9' W) for 2018 obtained from the Ocean Productivity repository (Oregon State University; http://sites.science.oregonstate.edu/ocean.productivity), quantified from MODIS-based remote sensing estimates of ocean surface chlorophyll a concentrations using the Vertically Generalized Production Model (VGPM; Behrenfeld & Falkowski 1997). Note that the obtained NPP values were averaged per month and for the whole 2018 to better highlight seasonal variabilities. (b) Flux of particulate organic carbon (POC) reaching the summit of the seamount from export of NPP estimated after Suess (1980) together with the proportion of POC burial (after Dunne et al. (2007)). The mean uptake rate for the coral garden in this study is expresses in mmol C m^{-2} d^{-1} assuming a 1:1 carbon to O_2 ratio (see Glud 2008).

Literature Cited

Behrenfeld MJ, Falkowski PG (1997) Photosynthetic rates derived from satellite-based chlorophyll concentration. Limnol Oceanogr 42:1–20

Berg P, Roy H, Wiberg PL (2007) Eddy correlation flux measurements: The sediment surface area that contributes to the flux. Limnol Oceanogr 52:1672–1684

Dunne JP, Sarmiento JL, Gnanadesikan A (2007) A synthesis of global particle export from the surface ocean and cycling through the ocean interior and on the seafloor. Global Biogeochem Cycles 21:Gb4006

Glud RN (2008) Oxygen dynamics of marine sediments. Mar Biol Res 4:243–289

Suess E (1980) Particulate Organic-Carbon Flux in the Oceans - Surface Productivity and Oxygen Utilization. Nature 288:260–263